Implementation of Photonuclear Reactions in UNIST Monte Carlo Code MCS

Matthieu Lemaire, Hyunsuk Lee, Douglas A. Fynan, Deokjung Lee*
Department of Nuclear Engineering, Ulsan National Institute of Science and Technology, 50, UNIST-gil, Ulsan, 44919, Republic of Korea
**Corresponding author: deokjung@unist.ac.kr*

1. Introduction

The capability to simulate photonuclear reactions has been implemented in the MCS Monte Carlo code [1] under development at the Ulsan National Institute of Science and Technology. This new feature completes the coupled neutron-photon transport capability of MCS by enabling both the production of gamma photons by neutron interactions and the production of neutrons by photonuclear reactions (photoneutron production). The simulation of photonuclear reactions is turned off by default and can be turned on in the MCS input file with the keyword "<photonuclear> on </photonuclear>".

Photonuclear reactions are commonly applied in the fields of radiation shielding and nuclear safeguard. They are also important in criticality applications for reactors with heavy water moderator and/or beryllium reflector. They are characterized as threshold reactions, with an energy threshold to produce photoneutrons between 5 MeV and 9 MeV for most nuclides. For lighter nuclides, the kinematic threshold energies of (γ,n) reactions can be lower: 1.6659 MeV for ^{9}Be and 2.2259 MeV for ^{2}H.

The plan of this paper is as follows. First, an overview of the ACE photonuclear files available for MCS simulations is presented. Then, the implementation of the photonuclear reactions, the Russian roulette scheme for photoneutrons and the kinematics of the photoneutron in (γ,n) reactions are detailed. Finally, preliminary results are presented by calculating with MCS and MCNP6 the photoneutron yield of sources described in the literature and comparing the calculated results to measured data.

2. Photonuclear data and algorithms

2.1. Photonuclear ACE files

The "endf7u" ACE file (extension .70u) based on the ENDF/B-VII.0 library is available in the MCNP package [2]. This file contains photonuclear data for 157 nuclides. The only reaction available for 141 nuclides is the reaction (γ,anything) (MT=5). Photofission (MT=18) data is available for 6 nuclides: ^{235,238}U, ^{237}Np, ^{239,240}Pu, ^{241}Am. Photoneutron production data by means of MT=50 (γ,n) reaction or MT=29 (γ,n+2α) reaction is available for 7 nuclides: ^{2}H, ^{9}Be, ^{12}C, ^{16}O, ^{51}V, ^{180,183}W.

The "endf7u" ACE file does not contain neutron production data by means of MT=50 (γ,n) reaction for the nuclides ^{182,186}W (because of missing photoneutron angular distribution), so the ACE files from the TENDL-2017 library [3] (extension .17u) with explicit channels up to 30 MeV are adopted for those two nuclides instead.

2.2. Photon mean free path

The total macroscopic photon cross-section Σ_{tot} is calculated as the sum of the total macroscopic photo-atomic cross-section $\Sigma_{tot,PA}$ and of the total macroscopic photonuclear cross-section $\Sigma_{tot,PN}$:

$$\Sigma_{tot} = \Sigma_{tot,PA} + \Sigma_{tot,PN} \, . \quad (1)$$

The total macroscopic photo-atomic cross-section is summed up element-wise for all the elements in the material composition and the total macroscopic photonuclear cross-section is summed up nuclide-wise for all the nuclides in the material composition. The photon mean free path used to sample the distance to the next collision is then simply given as MFP = $1/\Sigma_{tot}$.

2.3. Forced photoneutron production scheme

The photonuclear cross-sections are always small (less than 5-6%) compared to the total photon (photo-atomic + photonuclear) cross-sections, thus causing analog simulations of photonuclear reactions to have large tally variance. The variance reduction scheme from the Serpent 2 code [4] is adopted for better efficiency. At each photon collision, the photon history is split into two parts: one part undergoes a photo-atomic collision and the other part undergoes a photonuclear reaction. The weight of the photo-atomic part *W'* is given in Eq. (2) where *W* is the weight of the incident photon:

$$W' = \left(1 - \frac{\Sigma_{tot,PN}}{\Sigma_{tot}}\right) W \, . \quad (2)$$

The different steps of the photonuclear part are detailed in the sub-sections 2.4 to 2.8.

2.4. Sampling of the collision nuclide

The collision nuclide selected for a photonuclear interaction is independent of the element that is selected in the photo-atomic part for a photo-atomic interaction. The probability of selecting the collision nuclide *nuc* for a forced photonuclear interaction with the incident photon of energy *E* is given by Eq. (3), where the index *nuc* runs over the nuclides composing the material, N_{nuc} is the nuclide density and $\sigma_{nuc,rea}(E)$ is the microscopic cross-section of the photonuclear reaction *rea* of nuclide *nuc* at the incident photon energy *E*.

$$P_{nuc}(E) = \frac{N_{nuc} \sum_{rea} \sigma_{nuc,rea}(E)}{\sum_{nuc}\left[N_{nuc} \sum_{rea} \sigma_{nuc,rea}(E)\right]} \, . \quad (3)$$

Only the photonuclear reactions that can produce photoneutrons are forced in MCS. Thus, for each nuclide, the index *rea* only includes the photonuclear reactions that are listed in the photonuclear ACE file in the MTRP field of the secondary-particle-production IXS block corresponding to photoneutron production (IPT=1). The denominator of the right-hand-side fraction of Eq. (3) corresponds to the macroscopic photonuclear cross-sections of the forced photonuclear reactions and is rewritten in Eq. (4) for emphasis.

$$\Sigma_{PN,forced-reactions}(E) = \sum_{nuc}\left[N_{nuc}\sum_{rea}\sigma_{nuc,rea}(E)\right]. \quad (4)$$

2.5. Sampling of the photonuclear reaction

After the collision nuclide *nuc* has been selected, the photonuclear reaction *rea* is selected with the probability expressed in Eq. (5).

$$P_{rea}(E) = \frac{\sigma_{nuc,rea}(E)}{\sum_{rea}\sigma_{nuc,rea}(E)}. \quad (5)$$

2.6. Statistical weight of the photoneutron

One single photoneutron particle is created in MCS after each photonuclear reaction. The statistical weight W_n of this photoneutron particle is given by Eq. (6) where $\nu_{nuc,rea,n}(E)$ is the photoneutron multiplicity (number of emitted photoneutrons) for the reaction *rea* of nuclide *nuc* at the incident photon energy *E*.

$$W_n = \nu_{nuc,rea,n}(E)\frac{\Sigma_{PN,forced-reactions}(E)}{\Sigma_{tot}(E)}W. \quad (6)$$

This expression of the weight ensures the simulation remains unbiased ("fair game" simulation) by accounting both for the splitting of the photon history at collision into a photo-atomic part and a photonuclear part and for the photonuclear reactions that have been neglected because they do not produce photoneutrons.

In photonuclear ACE files, for each reaction included in the neutron-production (IPT=1) IXS block, the SIGP block contains the photoneutron yield data used to compute the neutron multiplicity $\nu_{nuc,rea,n}(E)$. The data is present in two different forms: MF=6, 12 or 16 where the direct multiplicity is tabulated; and MF=13 where the neutron production cross-section (multiplicity times cross-section) is given, requiring to compute the ratio of the neutron production cross section by the cross section to access the neutron multiplicity.

2.7. Russian roulette of photoneutrons

To reduce the variance of photoneutron-related tallies, photoneutrons are rouletted at birth and after each photoneutron collision to remove the photoneutrons with too low statistical weights. The photoneutron Russian roulette is played with lower weight $q \times W_L$ and survival weight $q \times W_S$, where W_L = 0.25 and W_S = 0.5 correspond to the values of the default neutron Russian roulette and the factor q equals 0.1 by default. This means that by default, the photoneutron Russian roulette is played with weights 10 times smaller than the default neutron Russian roulette in order to account for the inherently smaller weights of the photoneutrons compared to the population of other neutrons. The user may modify the value of q in the MCS input ($0 < q \leq 1$) with the keyword <roulette-factor-photoneutron> 0.1 </roulette-factor-photoneutron>.

2.8. Photoneutron kinematics

The relativistic kinematics described in [5] for the photoneutron production from (γ,n) reactions is adopted in MCS to model the properties of outgoing photoneutrons when the energy law LAW=33 "level scattering" is specified in the photonuclear ACE files. We note E_G the energy of the incident photon, m_N the mass of a neutron, m_T the mass of the target nuclide, m_R the mass of the residual nuclide, c the speed of light in vacuum. The total energy E'_N of the photoneutron in the center-of-mass system is given in Eq. (7) where s is the four-momentum Lorentz invariant given in Eq. (8). The mass of the residual nuclide is calculated in Eq. (9) using the Q-value of the reaction readily available in the photonuclear ACE files.

$$E'_N = \frac{sc^2 + (m_N c^2)^2 - (m_R c^2)^2}{2\sqrt{sc^2}}; \quad (7)$$

$$sc^2 = (m_T c^2)^2 + 2m_T c^2 E_G; \quad (8)$$

$$m_R c^2 = (m_T - m_N)c^2 - Q. \quad (9)$$

For all the photoneutrons, the conversion of the energy and direction of the photoneutron from the center-of-mass system to the laboratory system is done assuming that the photoneutrons are produced from a (γ,n) reaction. Under that hypothesis, the kinetic energy T_N of the photoneutron in the laboratory system is given in Eq. (10) where β expressed in Eq. (11) is the ratio of the center-of-mass velocity to the speed of light in vacuum, p' expressed in Eq. (12) is the momentum of the photoneutron in the center-of-mass system and μ' is the cosine of the polar angle between the incident photon direction and the photoneutron direction in the center-of-mass system.

$$T_N = \frac{E'_N + \beta p' c\mu'}{\sqrt{1-\beta^2}} - m_N c^2; \quad (10)$$

$$\beta = E_G/(E_G + m_T c^2); \quad (11)$$

$$p'c = \sqrt{(E'_N)^2 - (m_N c^2)^2} \quad (12)$$

The cosine μ of the polar angle between the incident photon direction and the photoneutron direction in the

laboratory system is given in Eq. (13) where $p_{\parallel}$ and $p_{\perp}$ are respectively the parallel and perpendicular components (with regards to the incident photon direction) of the photoneutron momentum in the center-of-mass system, expressed in Eq. (14) and Eq. (15). The azimuthal angle for the photoneutron direction is sampled uniformly in the interval [0:2π].

$$\mu = \frac{p_{\parallel} c}{\sqrt{(p_{\parallel} c)^2 + (p_{\perp} c)^2}} \; ; \tag{13}$$

$$p_{\parallel} c = (p' c \mu' + \beta E'_N)/\sqrt{1-\beta^2} \; ; \tag{14}$$

$$p_{\perp} \mathrm{c} = p' c \sqrt{1-\mu'^2} \, . \tag{15}$$

3. Preliminary results

The reference [6] describes experimental photoneutron yields for several neutron sources made of a gamma-emitter core (radius Ri = 0.5 cm) wrapped in a thin-walled tin plate container (thickness ≃ 0.01 cm, density = 7.265 g/cm^3) and surrounded by a sphere of target material of external radius Re. Two target materials are employed: beryllium, of density ρ = 1.73 g/cm^3 and purity > 99.7%, or heavy water, of density ρ = 1.107 g/cm^3 and purity > 99.8%. The source geometry is shown in Fig. 1.

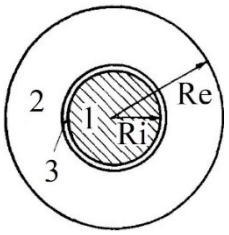

Fig. 1. Neutron source geometry. 1/ γ-emitter core; 2/beryllium or heavy water; 3/tin plate. [6]

The experimental results are presented under the form of "Wattenberg constants" μ^{eff} defined by Eq. (16) and expressed in units [s^{-1}.cm^2.g^{-1}.curie^{-1}]:

$$\mu_{EXP}^{eff} = \frac{Q}{4\pi\rho \mathrm{LA}} \; ; \tag{16}$$

where Q [s^{-1}] is the number of neutrons emitted per second by the source, ρ [g/cm^3] is the density of the target material, A is the activity of the γ-emitter core in units curie (1 curie = 3.7x10^{10} Bq) and L [cm] is a geometrical factor tabulated in Table I for different values of the external radius Re. The experimental results are summarized in Table II with reported uncertainties at one standard deviation.

Regarding the core material, antimony (Sb, ρ = 6.697 g/cm^3), indium (In, ρ = 7.31 g/cm^3) and gallium (Ga, ρ = 5.91 g/cm^3) are modelled in elemental form, whereas lanthanum (La) is modelled as La_2O_3 (ρ = 6.51 g/cm^3) and sodium (Na) is modelled as NaF (ρ = 1.26 g/cm^3). The gamma radioactivity of the spherical core is assumed homogeneous and isotropic. The energies and yields of the gamma photons emitted by the γ-emitter nuclides are tabulated in Table III according to the Nudat2.8 database [7]. Only the decay gamma energies above the (γ,n) threshold of the target material (beryllium or deuterium) and of yield > 0.1% are considered.

Table I: Values of the geometrical factor L for Ri = 0.5 cm and different values of Re [6]

Re [cm]	1.0	1.6	2.0	2.5
L [cm]	0.573	1.19	1.60	2.11

Table II: Experimental values of the Wattenberg constants for several source configurations [6]

Re [cm]	γ-emitter nuclide / target material	μ_{EXP}^{eff}
1.0	^{124}Sb / Be	1.026x10^5 ± 2.4%
1.6	^{124}Sb / Be	1.046x10^5 ± 2.4%
2.0	^{124}Sb / Be	1.047x10^5 ± 2.4%
2.5	^{124}Sb / Be	1.032x10^5 ± 2.4%
2.5	^{116m}In / Be	8.25x10^3 ± 3.5%
2.5	^{140}La / Be	1.81x10^3 ± 4.6%
2.5	^{24}Na / Be	1.013x10^5 ± 2.4%
2.5	^{24}Na / D_2O	2.209x10^5 ± 2.4%
2.5	^{72}Ga / D_2O	3.065x10^4 ± 2.4%

Table III: Energies and yields of gamma rays of interest [7]

γ-emitter nuclide	Energy (MeV)	Yield (number of photons per decay)
^{124}Sb	1.690971	0.4757
	2.090930	0.0549
^{116m}In	1.75250	0.0236
	2.11229	0.1509
^{140}La	2.34788	0.0085
	2.52140	0.0346
	2.54734	0.00101
^{24}Na	2.754007	0.99855
^{72}Ga	2.491026	0.0773
	2.507718	0.1333
	2.515857	0.00258
	2.621279	0.00141
	2.844160	0.00446

For each case, 30 million photon histories are simulated with MCS and MCNP6 in coupled neutron-photon transport mode with photonuclear reactions turned on. EPICS2014 photo-atomic data, 'endf7u' photonuclear data and ENDF/B-VII.1 neutron-transport data are employed. The neutron current *Cn* crossing the spherical surface of radius Re is tallied (F1 tally in MCNP), in units neutrons per photon source. The Wattenberg constants can then be determined as in Eq. (17) where Y [s^{-1}.curie^{-1}] is the number of gamma photons above the (γ,n) threshold energy of the target material emitted per second by one curie of gamma-emitter nuclide (i.e. Y = number of decay photons per 3.7x10^{10} decays).

$$\mu_{CODE}^{eff} = \frac{1}{4\pi\rho \mathrm{L}} C_n Y \, . \tag{17}$$

The results calculated by MCS with statistical uncertainties at one standard deviation and the calculation/experiment (C/E) ratios are given in Table IV. The results calculated by MCNP6 with statistical uncertainties at one standard deviation and the calculation/calculation (C/C) ratios are given in Table V. A systematic overestimation of the neutron source strength by ~2% for the beryllium target cases and ~16% for the heavy water target cases is observed for MCNP6 compared to MCS results. The systematic overestimation is likely due to the implementation of (γ,n) photoneutron kinematics in MCNP, which is reportedly incorrect and produces too hard photoneutron spectrum, especially for light nuclide target [5], thus leading to greater photoneutron mean free paths and more photoneutron leakage from the source. Agreement within 20% is observed between MCS and experimental values for 7 sources. Very notable disagreement is observed for the indium/beryllium source (C/E = +72.1%) and lanthanum/beryllium source (C/E = +152.0%), although MCS and MCNP6 give results within 2% for these two cases.

Table IV: Values of the Wattenberg constants calculated with MCS and (C/E) comparison

Re/core/target	μ_{MCS}^{eff}	$\mu_{MCS}^{eff}/\mu_{EXP}^{eff} - 1$
1.0/^{124}Sb/Be	1.172x10^5 ± 0.5%	+14.2% ± 2.4%
1.6/^{124}Sb/Be	1.159x10^5 ± 0.3%	+10.8% ± 2.4%
2.0/^{124}Sb/Be	1.144x10^5 ± 0.3%	+9.2% ± 2.4%
2.5/^{124}Sb/Be	1.124x10^5 ± 0.3%	+8.9% ± 2.4%
2.5/^{116m}In/Be	1.420x10^4 ± 0.4%	+72.1% ± 3.5%
2.5/^{140}La/Be	4.561x10^3 ± 0.4%	+152.0% ± 4.6%
2.5/^{24}Na/Be	8.390x10^4 ± 0.4%	-17.2% ± 2.4%
2.5/^{24}Na/D_2O	1.913x10^5 ± 0.3%	-13.4% ± 2.4%
2.5/^{72}Ga/D_2O	3.050x10^4 ± 0.4%	-0.5% ± 2.4%

Table V: Values of the Wattenberg constants calculated with MCNP6 and (C/C) comparison

Case	μ_{MCNP}^{eff}	$\mu_{MCNP}^{eff}/\mu_{MCS}^{eff} - 1$
1.0/^{124}Sb/Be	1.181x10^5 ± 1.5%	+0.8% ± 1.6%
1.6/^{124}Sb/Be	1.178x10^5 ± 1.0%	+1.7% ± 1.1%
2.0/^{124}Sb/Be	1.157x10^5 ± 0.9%	+1.2% ± 0.9%
2.5/^{124}Sb/Be	1.140x10^5 ± 0.8%	+1.4% ± 0.8%
2.5/^{116m}In/Be	1.442x10^4 ± 1.3%	+1.5% ± 1.3%
2.5/^{140}La/Be	4.639x10^3 ± 1.1%	+1.7% ± 1.2%
2.5/^{24}Na/Be	8.547x10^4 ± 1.3%	+1.9% ± 1.3%
2.5/^{24}Na/D_2O	2.210x10^5 ± 1.0%	+15.5% ± 1.0%
2.5/^{72}Ga/D_2O	3.545x10^4 ± 1.1%	+16.2% ± 1.2%

4. Conclusions and perspectives

Photonuclear reactions have been implemented in the Monte Carlo code MCS under development at the Ulsan National Institute of Science and Technology. A forced-collision scheme that produces one photoneutron particle per photon collision is adopted for improved variance of photoneutron-related tallies. Photoneutron kinematics is treated fully relativistically for the (γ,n) reaction. Reasonable results of neutron source strength are presented for 9 experimental photoneutron source configurations with 5 γ-emitter nuclides and 2 target materials.

Photonuclear benchmarks for future MCS validation studies are detailed in [2] and [8], the latter reference also containing several examples of MCNP inputs. However, those benchmarks involve electron sources and require electron transport, which is not available at the time in MCS. A workaround under consideration is to compute a bremsstrahlung photon source with a third-party code and to use it as a fixed photon source in neutron-photon transport mode in MCS.

Acknowledgment

This work was supported by the National Research Foundation of Korea (NRF) grant funded by the Korea government (MSIT). (No. NRF-2019M2D2A1A03058371).

REFERENCES

[1] H. Lee et al., "MCS – A Monte Carlo Particle Transport Code for Large-Scale Power Reactor Analysis," Annals of Nuclear Energy, 139: 107276 , 2020.
[2] M. Frankl et al., "Photonuclear Benchmarks of C, Al, Cu, Ta, Pb, and U from the ENDF/B-VII Cross-Section Library ENDF7U Using MCNPX", Nuclear Science and Engineering, 183:1, 135-142, 2016.
[3] Paul Scherer Institute, TENDL-2017 online repository, retrieved 2020, July 16, link: https://tendl.web.psi.ch/tendl_2017/tendl2017.html.
[4] T. Kaltiaisenaho, "Photonuclear reactions in SERPENT 2 Monte Carlo code", Proceeding M&C 2019, Portland, Oregon, Aug 25-29, 2019.
[5] E. Caro, "Relativistic kinematics for photoneutron production in Monte Carlo transport calculations," Annals of Nuclear Energy, 96: 170-175, 2016.
[6] F. Bensch et al., "Yields and spectra of some spherical photoneutron sources," Journal of Nuclear Energy, 23: 537-550, 1969.
[7] Brookhaven National Laboratory, National Nuclear Data Center, NuDat 2.8 database, retrieved 2020, July 3, link: https://www.nndc.bnl.gov/nudat2/.
[8] M. C. White, "Development and implementation of photonuclear cross-section data for mutually coupled neutron-photon transport calculations in the Monte Carlo N-Particle (MCNP) radiation transport code", thesis, LA-13744-T, University of Florida, July 2000